Acta Crystallographica Section D
Biological Crystallography
ISSN 0907-4449

Structure of FKBP12.6 in complex with rapamycin

Champion C. S. Deivanayagam, Mike Carson, Aruna Thotakura, Sthanam V.L. Narayana and Ramarao S. Chodavarapu*

Center for Macromolecular Crystallography, School of Optometry, 250 BHSB, 1918 University Boulevard, Birmingham, AL 35294-0005, USA

Correspondence e-mail: ramarao@uab.edu

Received 5 August 1999
Accepted 22 December 1999

PDB Reference: rapamycin–FKBP12.6 complex, 1c9h.

FKBP12.6 is a novel isoform of FKBP12, which selectively binds to the cardiac ryanodine receptor (RyR2). The crystal structure of FKBP12.6 in complex with rapamycin has now been determined at 2.0 Å resolution. The structures of FKBP12.6 and FKBP12 are nearly identical, except for a displacement observed in the helical region of FKBP12.6 toward the hydrophobic pocket. This displacement was not predicted by homology modeling studies. Analyses of the residues that are likely to confer the RyR2-binding specificity are presented.

1. Introduction

FK506 is a potent immunosuppressive drug that binds to a family of related intracellular receptors termed FK506-binding proteins (FKBPs) and varying in size from 12 to 54 kDa (Wiederrecht & Etzkorn, 1994). FKBP12 mediates the immunosuppressive action of FK506 in T lymphocytes by blocking a key step required in the activation of transcription factors (NF-AT, AP3 and NF-κB) which promote expression of lymphokine genes such as interleukin-2 (IL-2; Crabtree, 1989). The immunosuppressive action of the drug is related to its inhibition of calcineurin, a calcium-dependent protein phosphatase involved in intracellular signal transduction, by binding to FKBP (Liu *et al.*, 1991; Sewell *et al.*, 1994; Lam *et al.*, 1995); Kissinger *et al.* (1995) have reported the crystal structure of human FKBP12–FK506–calcineurin complex. All known FKBP family members display *cis–trans* peptidyl–prolyl isomerase (PPIase) activity that is inhibited by FK506 and a structurally related compound, rapamycin (Wiederrecht & Etzkorn, 1994).

In skeletal muscle and heart, the ryanodine receptor (RyR)/calcium-release channel serves to release Ca^{2+} from sarcoplasmic reticulum, thereby triggering muscle contraction (Fleischer & Inui, 1989; McPherson & Campbell, 1993; Meissner, 1994). FKBP12 has been found to be tightly associated with skeletal muscle RyR (RyR1) and more recently its novel isoform FKBP12.6 was found to be selectively associated with cardiac RyR (RyR2; Jayaraman *et al.*, 1992; Timerman *et al.*, 1993, 1994). A number of functional similarities are observed between FKBP12 and FKBP12.6. These include a 85% sequence identity, PPIase activity that is inhibited by both FK506 and rapamycin, and inhibition of calcineurin when ternary complexes are formed with FKBP and FK506 (Liu *et al.*, 1991; Sewell *et al.*, 1994; Lam *et al.*, 1995).

FKBP12.6 has been suggested to be involved in the regulation of insulin biosynthesis and secretion by modulating intracellular Ca^{2+} levels *via* RyR2 in rat pancreatic islets (Barg

et al., 1997). The precise role of FKBP12.6 in cardiac excitation–contraction coupling and insulin secretion remains to be elucidated. Recently, three amino-acid residues, Gln31, Asn32 and Phe59, were identified through site-directed mutagenesis studies and were reported to be involved in the selective binding of the FKBP12.6 to the RyR2 receptor (Xin *et al.*, 1999).

The first crystal structures of human FKBP12 complexes with rapamycin were reported by Van Duyne *et al.* (1993). In this paper, we present the crystal structure of FKBP12.6 in complex with rapamycin and analyze the residues implicated in the selective binding of RyR2.

2. Methods

2.1. Generation of human FKBP12.6 cDNA

Complementary DNA encoding the human FKBP12.6 was generated from human brain single-stranded DNA by PCR. The published FKBP12.6 sequence (Lam *et al.*, 1995; Arakawa *et al.*, 1994) was used for the design of the primers. The sense primer corresponding to FKBP12.6 was synthesized with a *Bam*H1 site at the 5′ end. Similarly, the antisense primer has a *Hin*dIII site at the terminus. The sequences of the primers are as follows: sense, ATT GGA TCC ATG GGC GTG GAG ATC GAG ACC; antisense, ATT AAG CTT TCA CTC TAA GTT GAG CAG CTC.

'Gene Pool' human brain single-stranded DNA was obtained from Invitrogen and used as a template. 100 pmol of each primer and 0.5 µg of SSDNA were used in the PCR reaction. The PCR was performed for 30 cycles (365 K denaturing for 30 s, 333 K annealing for 30 s and 345 K extension for 2 min). The PCR product was purified on an agarose gel, digested with *Bam*H1 and *Hin*dIII enzymes and cloned into pET23A vector (Novagen), which was previously digested with the same enzymes and purified. Plasmid DNA was sequenced to establish the identity of the insert and then transformed into *Escherichia coli* (BL21 DE3pLysS).

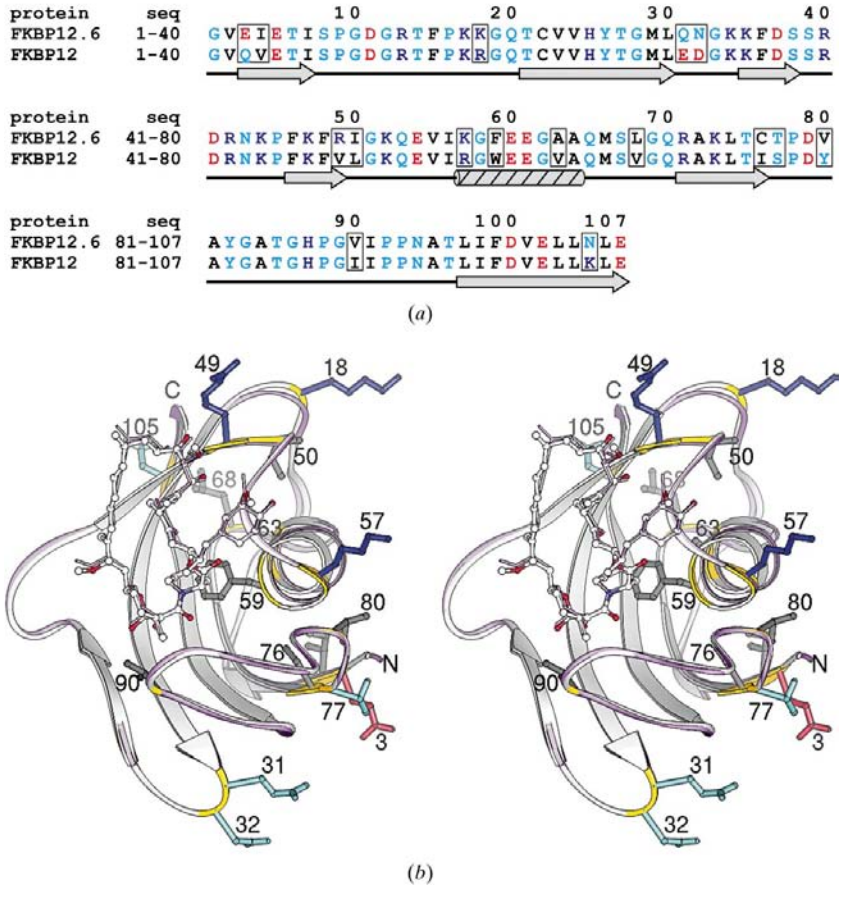

Figure 1
(*a*) Sequence alignment and secondary structure of FKBP12.6 and FKBP12. Red, blue, cyan and black letters represent the negative, positive, polar and hydrophobic residues, respectively. The non-identical residues are boxed. Arrows, cylinders and lines represent sheets, helices and coils. (*b*) Stereo diagram of the superposition of the rapamycin complexes of FKBP12.6 (white) and FKBP12 (lavender). The superposition is based on all 107 C^{α} atoms. The ribbon and rapamycin bonds for FKBP12 are thinner. Yellow marks the non-identical residues on the FKBP12.6 ribbon and their side chains are shown colored by type as in (*a*): red, negative; blue, positive; cyan, polar; gray, hydrophobic.

2.2. Purification of recombinant FKBP12.6

E. coli cells containing the FKBP12.6 pET23 plasmid were induced with 1 m*M* IPTG and the protein was purified, essentially as described by Lam *et al.* (1995). Bacteria producing the recombinant protein were pelleted and resuspended in 5 m*M* phosphate buffer (pH 6.8) containing 1 m*M* EDTA and 5 m*M* β-mercaptoethanol. The suspension was freeze-thawed three times and the soluble proteins were collected by centrifugation. FKBP12.6 was purified on a CM cellulose (Pharmacia) column in a single step.

2.3. Crystallization of FKBP12.6

Crystals of FKBP12.6 were grown using the hanging-drop vapor-diffusion method and the screening of crystallization conditions was performed with the Hampton crystal-screening kit. A droplet consisting of 2 µl of protein at a concentration of 8 mg ml^{-1}, 2 µl of the well solution and 2 µl of rapamycin (14 µ*M*) in methanol was equilibrated against 1 ml of the well solution (reservoir). The well solution consisted of 40% PEG 4000 [50%(*w*/*v*)], 0.2 *M* lithium sulfate and 0.1 *M* HEPES buffer (pH 7.4). Thick rod-shaped crystals grew in 7–10 d to dimensions of 0.4 × 0.15 × 0.1 mm.

2.4. X-ray data collection

Crystals were dropped into a cryo-solution containing 15% glycerol and immediately picked up and flash-frozen at 100 K and exposed to X-rays. Data were recorded using an R-AXIS IV image-plate detector mounted

on a Rigaku HU-3R rotating-anode generator operating at 100 mA and 50 kV. X-ray diffraction data to a resolution of 2.0 Å were collected over 144 frames (1° oscillations, crystal-to-detector distance of 150 mm and 20 min exposure time). The frames were indexed and scaled using *DENZO* and *SCALEPACK* (Otwinowski, 1993). The crystallographic data is summarized in Table 1.

2.5. Structure determination and refinement

Rigid-body refinements with the initial polyalanine model of FKBP12 (1fkl) in the resolution range 8.0–4.0 Å were carried out using *X-PLOR* (Brünger, 1996). The initial $R_{\rm free}$ and R factors for this model were 41.9 and 40.9%, respectively, and after further positional refinement the model had $R_{\rm free}$ and R factors of 49.2 and 24.5%, respectively. Side chains and rapamycin were added to this newly oriented model and after further positional refinements the model had $R_{\rm free}$ and R factors of 42.9 and 26.3%, respectively, in the resolution range 8.0–3.0 Å resolution. This model was subsequently refined using the automated refinement procedure *ARP* (Perrakis *et al.*, 1999) and after 30 cycles of refinement the $R_{\rm free}$ and R factors dropped to 29.9 and 25.9%, respectively. Model building to fit the electron density was carried out with the graphics program *O* (Jones *et al.*, 1991) in conjunction with *OOPS* (Kleywegt & Jones, 1997), thereby keeping a constant check on the quality of the model. The last few cycles of refinement were carried out using *CNS* (Adams *et al.*, 1997) while applying the bulk-solvent correction. All reflections ($\geq 2\sigma$) in the resolution range 20.0–2.0 Å were used in refinement, with 10% partitioned in a test set for monitoring the refinement process (Brünger, 1992). With 101 water molecules, the model was refined to final $R_{\rm free}$ and R factors of 23.9 and 20.0%, respectively. The final refinement results are listed in Table 1.

Table 1
Crystallographic data of FKBP12.6.

Unit-cell parameters	
a (Å)	45.70
b (Å)	49.29
c (Å)	51.69
$\alpha = \beta = \gamma$ (°)	90.00
Space group	$P2_12_12_1$
Resolution (Å)	2.0
$I/\sigma(I)$	17.8
$R_{\rm sym}$† (%)	6.5
V_m (Å^3 Da^{-1})	2.3
No. of measured reflections	105747
No. of unique reflections	7941
Reflections >3σ (last shell, %)	86.7
Completeness (overall, %)	94.2
No. of molecules in asymmetric unit	1
R factor	20.04
$R_{\rm free}$	23.86
R.m.s.d. (bonds)	0.009
R.m.s.d. (angles)	1.488
Average B factor of protein (Å^2)	27.84
Average B factor, main chain (Å^2)	26.15
Average B factor, side chain (Å^2)	29.70
No. of solvent molecules	101

† $R_{\rm sym} = \sum |I_h - \langle I_h \rangle| / \sum I_h$, where $\langle I_h \rangle$ is the average intensity over symmetry equivalents.

The final model was examined for main-chain torsion angles (φ, ψ) using *PROCHECK* (Laskowski *et al.*, 1993); the Ramachandran plot shows 88.4% of non-glycine residues in the most favored regions and a further 10.5% in the allowed region. Only one residue, Ala81, is found in the generously allowed region with a well defined electron density. Similar (φ, ψ) values have been observed for Ala81 in other FKBP12 structures. The final model fits the electron density well, except for the first N-terminal residue, Met0, which could not be located on the map (the residue numbering is based on FKBP12 for ease of comparison).

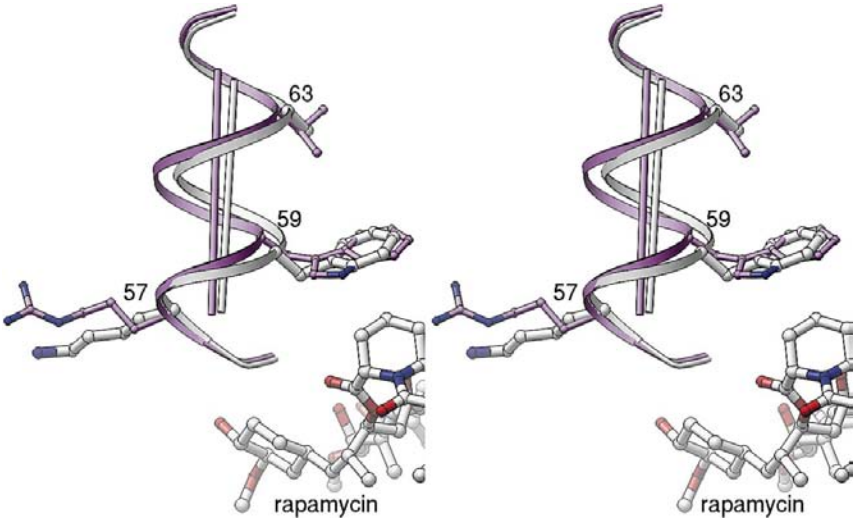

Figure 2
Stereo diagram of the helices of FKBP12.6 (white) and FKBP12 (lavender), with their respective helical axes. The superposition is as in Fig. 1(*b*), based on all C$^\alpha$s. The axes are fit to the C$^\alpha$s of residues 57–64. The axes are at a 4° angle and are shifted by 0.7 Å at their midpoint. The three mutated residues are shown as ball-and-sticks, with atoms colored red and blue for oxygen and nitrogen, respectively, and white or lavender for carbon.

3. Results and discussion

3.1. Overall structure

Wilson *et al.* (1995) have superposed different complex structures of FKBP12 and have reported that the helical and β-sheet regions are largely conserved, with variability found only in the loop regions. Their 1.7 Å FKBP12–rapamycin complex (PDB code 1fkl) will serve as the reference structure in the comparisons that follow. The overall structure of FKBP12.6 is very similar to FKBP12. The sequences are 85% identical and the structures superpose with an r.m.s.d. (on C$^\alpha$) of 0.47 Å (Fig. 1). The five β-strands form a sheet on one side of the molecule and the short helix spans three of these strands on the other side. Residues from the other strands, the helix and two loops form a hydrophobic surface pocket that binds rapamycin.

The hydrogen-bonding patterns between the proteins and rapamycin are identical in both FKBP12 and FKBP12.6. Based on the superposition of Fig. 1, the rapamycin coordinates of FKBP12.6 show a gradual shift up to 1.65 Å, starting from C12 and ending at C26, on the side that was shown to bind FRAP (Choi *et al.*, 1996). There is very little difference in main-chain conformations, except for a significant shift of the helix towards the β-sheet. The maximum main-chain displacement of up to 1.7 Å occurs near Glu60 and Phe59. Fig. 2 compares the helical regions. The key sequence substitutions of Phe59 (for Trp) and Ala63 (for Val) enable this displacement, while the hydrophobic face of the helix maintains tight packing with the sheet in the interior of the protein. Residue 59 is also crucial, as its side chain forms the floor of the hydrophobic pocket.

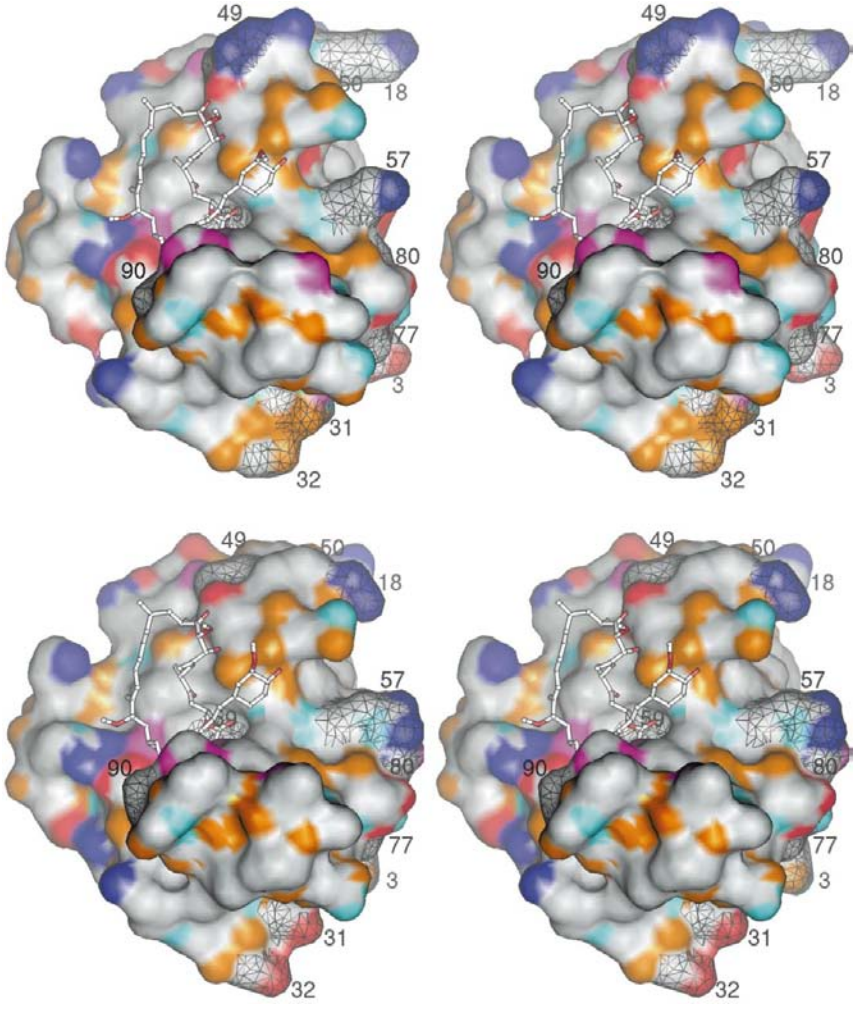

Figure 3
Stereo diagrams of the protein surfaces of rapamycin complexes of FKBP12.6 and FKBP12. The rapamycin is shown in ball-and-stick format, colored white, red and blue for carbon, oxygen and nitrogen, respectively. The protein surfaces are colored by chemical property: white is hydrophobic, red is negatively charged, blue is positively charged, orange is a hydrogen-bond acceptor, cyan is a hydrogen-bond donor and magenta can both accept and donate hydrogen bonds. Exposed surfaces of non-identical residues are textured with a mesh and labeled. The orientation is as in Fig. 1(*b*), only 90% smaller. Above, FKBP12.6; below, FKBP12.

3.2. Structure/function implications

FKBP12 binds RyR1 at a conserved Val-Pro peptide sequence (LSRL**VP**LDDLV), while FKBP12.6 binds RyR2 at a conserved Ile-Pro peptide sequence (LRSL**IP**LDDLV) (Cameron *et al.*, 1997). The specificity of binding is determined by the structures of the respective RyRs and the FKBPs. The crystal structures of neither RyR1 nor RyR2 are known at this time.

Xin *et al.* (1999) recently reported site-directed mutagenesis studies showing that three amino-acid residues, Gln31, Asn32 and Phe59, determine the selective binding of FKBP12.6 to the cardiac ryanodine receptor RyR2. They also created a homology model of FKBP12.6 using the *SWISS-MODEL* software (Guex & Peitsch, 1997). No major conformational changes were noted, but a larger hydrophobic pocket was observed in their FKBP12.6 model owing to the smaller size of the Phe substituted for Trp at residue 59.

We observe Gln31 and Asn32 as surface residues pointing away from the hydrophobic binding pocket. Both residues show clear electron density on a turn connecting the two strands whose interior residues help define the pocket. There is essentially no change between the structures in this region owing to the conversion of the acidic side chains to their respective amides. The Gln31 and Asn32 substitutions in FKBP12.6 yield a decrease of two negative charges compared with FKBP12 (Glu31, Asp32). Fig. 3 compares the surface chemical properties of FKBP and FKBP12.6. The view chosen maximizes the surface that has changed owing to the amino-acid substitutions between the two isoforms of the FKBP.

Xin *et al.* (1999) suggested that charge repulsion is a factor in the lack of binding of FKBP12 to RyR2. They also hypothesized that the larger hydrophobic binding pocket in their FKBP12.6 model would better accommodate the Ile in RyR2 compared with the smaller Val in RyR1. This is not supported by the present structural analysis. Fig. 4 presents comparisons of the hydrophobic pockets of the FKBP isoforms. The six-membered ring of Phe59 in FKBP12.6 is superposed on the six-membered ring of Trp59 in FKBP12, in the same plane (Figs. 2, 4). This maintains a very similar arrangement of the core aromatic residue side chains forming the binding pocket: Tyr26, Phe46, Phe48, Phe(Trp)59, Tyr82 and Phe99. The chemical properties of the hydrophobic pocket are nearly identical (Fig. 4). Surface

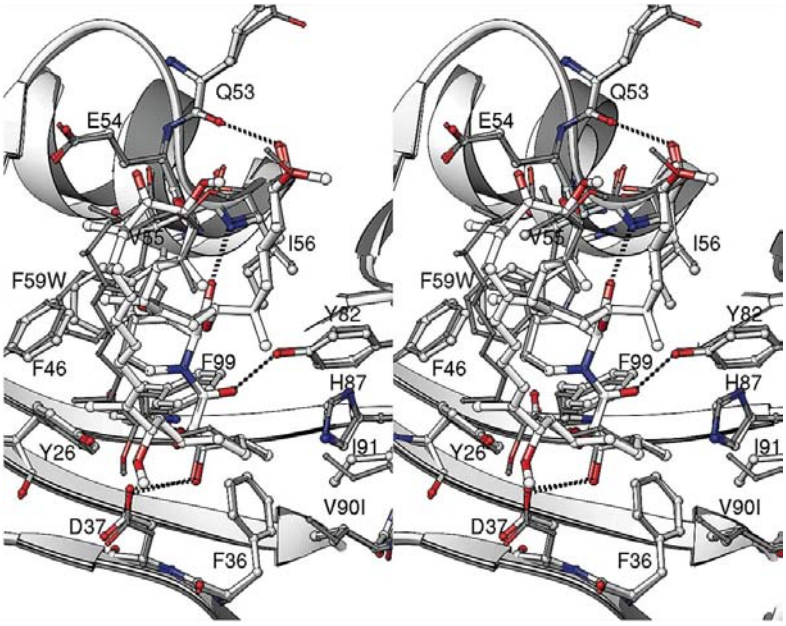

Figure 4
Stereo diagrams of the hydrophobic binding pockets of FKBP12.6 and FKBP12. All residues and surfaces within 4 Å of rapamycin are shown. Ribbons and carbon are white in FKBP12.6 and gray in FKBP12. O atoms and N atoms are red and blue, respectively, in both. Hydrogen bonds are shown as dashed black lines.

and volume calculations performed with *MSP* (Connolly, 1993) involving the respective proteins and 16 atoms of rapamycin occupying the base of the pocket estimated that the FKBP12.6 pocket is actually smaller than that of FKBP. The difference, however, is only 17 $Å^3$, a volume equivalent to that occupied by half a water molecule.

The suggestion of a larger pocket by Xin *et al.* (1999) would only be true if the helix were not displaced. We suggest the extra space required to bind the larger Ile in RyR2 (*versus* Val in RyR1) is made available by the substitution of the smaller Val90 in FKBP12.6 for Ile90 in FKBP12. Residue 90 is present at the edge of the hydrophobic pocket, on a loop just above residue 31 (see Figs. 3, 4). This is located near the C atoms in FK506 (and rapamycin) which were suggested to be a peptidomimetic to leucine for FKBP12 (Albers *et al.*, 1990) and also near the catalytic residue for the PPIase activity, His87.

4. Conclusions

The crystal structure of the FKBP12.6–rapamycin complex is very similar to that of the FKBP12–rapamycin complex of Wilson *et al.* (1995). However, a result unexpected from the molecular-modeling studies (Xin *et al.*, 1999) was the observed displacement of the entire helix owing to a concerted set of amino-acid substitutions. This underscores a limitation of automated homology modeling. Since all the previous crystal structures had similar main-chain conformation, their model also adhered to the same conformation. Apparently, current energy-minimization techniques are not able to effect such a large-scale shift of a secondary-structural element that results from multiple mutations.

In their site-directed mutagenesis study, Xin *et al.* (1999) began with a series of eight single mutations to test the most different substitutions between FKBP12.6 and FKBP12. However, from our structural results we speculate that two residues which were not tested might contribute to the specificity of RyR2 for FKBP12.6: Ala63 (from Val) and Val90 (from Ile). The former allows the entire helix (including Phe59) to shift, which maintains the hydrophobic core that forms the bottom of the binding pocket. The latter creates extra space on the edge of the pocket to accommodate the larger Ile-Pro presented by the cardiac ryanodine receptor RyR2. These speculations need confirmation by further mutagenesis studies. That such seemingly harmless substitutions of apolar residues could have such an effect reminds us again of the subtle beauty of protein structure.

CCSD thanks Vimal Shah and Dwight Moore for the discussions on crystallization. SVLN and CSR acknowledge the support for this project from NASA.

References

Adams, P. D., Pannu, N. S., Read, R. J. & Brünger, A. T. (1997). *Proc. Natl Acad. Sci. USA*, **94**, 5018–5023.
Albers, M. W., Walsh, C. T. & Schreiber, S. L. (1990). *J. Org. Chem.* **55**, 4984–4986.
Arakawa, H., Nagase, H., Hayashi, H., Fujiwara, T., Ogawa, M., Shin, S. & Nakamura, Y. (1994). *Biochem. Biophys. Res. Commun.* **200**, 836–843.
Barg, S., Copello, J. A. & Fleischer, S. (1997). *Am. J. Physiol.* **272**, C1726–1733.
Brünger, A. T. (1992). *Nature (London)*, **355**, 472–475.
Brünger, A. T. (1996). *X-PLOR Version 3.85. A System for X-ray Crystallography and NMR.* Yale University, New Haven, Connecticut, USA.
Cameron, A. D., Nucifora, F. C. Jr, Fung, E. T., Livingstone, D. J., Aldape, R. A., Ross, C. A. & Snyder, S. H. (1997). *J. Biol. Chem.* **272**, 27582–27588.
Carson, M. (1997). *Methods Enzymol.* **277**, 493–505.
Choi, J., Chen, J., Schreiber, S. L. & Clardy, J. (1996). *Science*, **273**, 239–241.
Crabtree, B. R. (1989). *Science*, **243**, 355–361.
Connolly, M. L. (1993). *J. Mol. Graph.* **11**, 139–141.
Fleischer, S. & Inui, M. (1989). *Annu. Rev. Biophys. Chem.* **18**, 333–364.
Guex, N. & Peitsch, M. C. (1997). *Electrophoresis*, **18**, 2714–2723.
Jayaraman, T., Brillantes, A. M., Timerman, A. P., Fleischer, S., Erdjument-Bromage, H., Tempst, P. & Marks, A. R. (1992). *J. Biol. Chem.* **267**, 9474–9477.
Jones, T. A., Zou, J. Y., Cowan, S. W. & Kjeldgaard, M. (1991). *Acta Cryst.* A**47**, 110–119.
Kissinger, C. R., Parge, H. E., Knighton, D. R., Lewis, C. T., Pelletier, L. A., Tempczyk, A., Kalish, V. J., Tucker, K. D., Showalter, R. E., Moomaw, E. W., Gastinel, L. N., Habuka, N., Chen, X., Mldonado, F., Barker, J. E., Bacuet, R. & Villafranca, J. E (1995). *Nature (London)*, **378**, 641–644.
Kleywegt, G. J. & Jones, T. A. (1997). *Methods Enzymol.* **276**, 208–330.

Lam, E., Martin, M. M., Timerman, A. P., Sabers, C., Fleischer, S., Lukas, T., Abraham R. T., O'Keefe, S. J., O'Neill, E. A. & Wiederrecht, G. J. (1995). *J. Biol. Chem.* **270**, 26511–26522.
Laskowski, P. A., MacArthur, M. W., Hutchinson, S. G. & Thornton, J. M. (1993). *J. Appl. Cryst.* **26**, 283–291.
Liu, J., Farmer, J., Lane, W., Friedman, J., Weissman, I. & Schreiber, S. (1991). *Cell*, **66**, 807–815.
McPherson, P. S. & Campbell, K. P. (1993). *J. Biol. Chem.* **268**, 13765–13768.
Matthews, B. W. (1968). *J. Mol. Biol.* **33**, 491–497.
Meissner, G. (1994). *Annu. Rev. Physiol.* **56**, 485–508.
Otwinowski, Z. (1993). *DENZO. A Film Processing Program for Macromolecular Crystallography*. Yale University, New Haven, Connecticut, USA.
Perrakis, A., Morris, R. & Lamzin, V. S. (1999). *Nature Struct. Biol.* **6**, 458–463.
Sewell, T., Lam, E., Martin, M., Leszyk, J., Weinder, J., Calaycay, J., Griffin, P., Williams, H., Hung, S., Cryan, J., Sigal, N. & Wiederrecht, G. J. (1994). *J. Biol. Chem.* **269**, 21094–21102.
Timerman, A. P., Jayaraman, T., Wiederrecht, G., Onoue, H., Marks, A. R. & Fleischer, A. (1994). *Biochem. Biophys. Res. Commun.* **198**, 701–706.
Timerman, A. P., Ogunbumni, E., Freund, E., Wiederrecht, G., Marks, A. R. & Fleischer, S. (1993). *J. Biol. Chem.* **268**, 22992–22999.
Timerman, A. P., Onoue, H., Xin, H.-B., Barg, S., Copello, J., Wiederrecht, G. & Fleischer, S. (1996). *J. Biol. Chem.* **271**, 20385–20391.
Van Duyne, G. D., Standaert, R. F., Karplus, P. A., Schreiber, S. L. & Clardy, J. (1993). *J. Mol. Biol.* **229**, 105–124.
Wiederrecht, G. & Etzkorn, F. (1994). *Perspect. Drug Discov. Des.* **2**, 57–84.
Wilson, K. P., Yamashita, M. M., Sintchak, M. D., Rotstein, S. H., Murcko, M. A., Boger, J., Thomson, J. A., Fitzgibbon, M. J., Black, J. R. & Navia, M. R. (1995). *Acta Cryst.* D**51**, 511–521.
Xin, B.-H., Rogers, K., Qi, Y., Kanematsu, T. & Fleischer, S. (1999). *J. Biol. Chem.* **274**, 15315–15319.